Journal of Physics B: Atomic, Molecular and Optical Physics

How can a 22-pole ion trap exhibit ten local minima in the effective potential?

To cite this article: R Otto *et al* 2009 *J. Phys. B: At. Mol. Opt. Phys.* **42** 154007

View the article online for updates and enhancements.

Related content

- Radiofrequency multipole traps: tools for spectroscopy and dynamics of cold molecular ions
  Roland Wester
- About the dynamics and thermodynamics of trapped ions
  C Champenois
- Storage of protonated water clusters in a biplanar multipole rf trap
  C Greve, M Kröner, S Trippel et al.

Recent citations

- An analytical approach to symmetry breaking in multipole RF-traps
  M Marchenay *et al*
- Single-phase ion trap with cylindrical zero-potential surface
  I. Kosternoi *et al*
- Thermometry in a Multipole Ion Trap
  Markus Nötzold *et al*

IOP ebooks™

Bringing together innovative digital publishing with leading authors from the global scientific community.

Start exploring the collection–download the first chapter of every title for free.

This content was downloaded from IP address 141.51.197.22 on 01/06/2021 at 13:38

J. Phys. B: At. Mol. Opt. Phys. **42** (2009) 154007 (6pp) doi:10.1088/0953-4075/42/15/154007

How can a 22-pole ion trap exhibit ten local minima in the effective potential?

R Otto[1], P Hlavenka[1], S Trippel[1], J Mikosch[1,3], K Singer[2], M Weidemüller[1,4] and R Wester[1]

[1] Physikalisches Institut, Universität Freiburg, Hermann-Herder-Straße 3, 79104 Freiburg, Germany
[2] Institut für Quanteninformationsverarbeitung, Universität Ulm, Albert-Einstein-Allee 11, 89081 Ulm, Germany

E-mail: roland.wester@physik.uni-freiburg.de

Received 10 February 2009, in final form 17 March 2009
Published 15 July 2009
Online at stacks.iop.org/JPhysB/42/154007

Abstract
The column density distribution of trapped OH^- ions in a 22-pole ion trap is measured for different trap parameters. The density is obtained from position-dependent photodetachment rate measurements. Overall, agreement is found with the effective potential of an ideal 22-pole. However, in addition, we observe ten distinct minima in the trapping potential, which indicate a breaking of the 22-fold symmetry. Numerical simulations show that a displacement of a subset of the radiofrequency electrodes can serve as an explanation for this symmetry breaking.

(Some figures in this article are in colour only in the electronic version)

1. Introduction

Multipole radiofrequency ion traps [1], in particular the 22-pole ion trap [2], are versatile devices used in laser spectroscopy [3–10] and investigations of chemical reaction processes [2, 11–13] of atomic and molecular ions. High-order multipole traps offer a large field-free region in the trap centre, and therefore provide a reduced interaction time of the ions with the oscillating electric field compared to a quadrupole trap [14]. Buffer gas cooling down to cryogenic temperatures of the translational [3, 7], rotational [3, 9] and vibrational degrees of freedom [8] of trapped molecular ions has been demonstrated. This enables applications with all the advantages of low-temperature experiments, such as a reduced Doppler width in spectroscopy studies and a well-defined population of internal states.

Stable confinement of a single ion in the oscillating quadrupole field of a Paul trap is precisely predicted, because the Mathieu equations of motion can be solved analytically. This is different for oscillating high-order multipole fields, where the equations of motion have no analytical solution. However, the movement of the ions in a fast-oscillating rf field justifies the assumption of an effective trapping potential, based on the separation of the ion motion into a smooth drift and a rapid oscillation, called micromotion [15]. This effective potential can be expressed as

$$V^*(\vec{r}) = \frac{1}{4}\frac{(q\vec{E}(\vec{r}))^2}{m\Omega^2} + q\Phi_0, \tag{1}$$

where $\vec{E}(\vec{r})$ denotes the electric field at the point $\vec{r}$, m is the mass of a test particle with charge q in an electric field oscillating on frequency Ω, and Φ_0 is a non-oscillating dc potential. For an ideal cylindrical multipole of order n this effective potential can be expressed as

$$V^*(r) = \frac{1}{4}\frac{n^2(qV_0)^2}{m\Omega^2 r_0^2}\left(\frac{r}{r_0}\right)^{2n-2}, \tag{2}$$

where V_0 denotes the amplitude of the oscillating rf field. For a high-order multipole field ($n = 11$ for the 22-pole trap) this creates an almost box-like trapping volume with steep walls and a large field-free region in the centre. This is important to suppress rf heating when cooling ions in neutral buffer gas [14].

The number of trapped ions that can be excited with radiation depends on the local density of ions in the interaction volume with the light field. In experiments with trapped

[3] Present address: National Research Council Canada, 100 Sussex Drive, Ottawa, ON K1A 0R6, Canada.
[4] Present address: Physikalisches Institut, Universität Heidelberg, Philosophenweg 12, 69120 Heidelberg, Germany.

 © 2009 IOP Publishing Ltd Printed in the UK

Ba^+ ions in an octupole trap the density has been imaged by spatially resolving the fluorescence signal [16, 17]. In this paper, we report on a method based on the photodetachment of trapped anions that allows us to image the density distribution of the trapped ions. In this way, we measure the experimental trapping potential of a 22-pole trap with unprecedented accuracy and study its dependence on the radiofrequency field. In the following section, the photodetachment tomography is explained, followed by a presentation of measured density distributions at different temperatures and rf amplitudes. We find ten unexpected maxima in the density distribution and analyse their origin with the help of numerical simulations in section 4.

2. Experimental procedure

The experimental radiofrequency ion trap setup has been described in detail in [18]. Its central element is a 22-pole trap [2] with good optical access along the trap axis. In the present tomography experiments, we have used an ensemble of stored OH^- anions cooled to a translational temperature of either 170 or 300 K. The use of negative ions allows us to perform photodetachment measurements, where the anions are depleted by a laser beam propagating parallel to the symmetry axis of the trap [19, 20]. The photodetachment process

$$OH^- + h\nu \rightarrow OH + e^-, \tag{3}$$

with $h\nu > 1.83$ eV, yields a depletion rate proportional to the photodetachment cross section and to the overlap of the ion column density with the photon flux. By scanning the position of the laser beam and measuring the depletion rate at each position the relative ion column density distribution is obtained. For small ion densities, where the Coulomb interaction between the ions can be neglected, the depletion rate at the transverse position (x, y) can be expressed as

$$k(x, y) = \sigma_{\mathrm{pd}} F_L \rho(x, y). \tag{4}$$

It depends only on the total photon flux F_L, the photodetachment cross section σ_{pd} and the single particle column density $\rho(x, y)$, reflecting the spatial overlap of the laser beam with the ion distribution [19]. As the latter is normalized to unity, we can write it as

$$\rho(x, y) = \frac{k(x, y)}{\int_S k(x, y)\,\mathrm{d}S}. \tag{5}$$

Thus, a full two-dimensional tomography scan of the trapped ions can be used to map the entire ion column density in the trap. If $k(x, y)$ is measured for the whole ion distribution, also the absolute photodetachment cross section can be obtained [20].

Ions are produced in a pulsed supersonic expansion of a suitable precursor gas, crossed by a 1 keV electron beam. For the OH^- production we use a mixture of $Ar/NH_3/H_2O$ (88%, 10%, 2%) to create NH_2^-. A rapid chemical conversion by water forms the OH^- anions in the source. A bunch of ~500 mass-selected ions is loaded into the trap, which is enclosed by a copper housing that is temperature variable between 8 and 300 K. A typical He buffer gas density of 1×10^{14} cm^{-3}, employed for all temperatures, is enhanced by a buffer gas pulse during the ion injection. The trap is operated with $\Omega = 2\pi \times 5$ MHz radiofrequency and different rf amplitudes. Along the axial direction, ions are confined by end electrodes biased to -2 V. To allow good thermalization of the ions, a storage period of 200 ms is inserted before the laser beam is switched on. After a given storage and laser interaction time the current signal, proportional to the number of ions that survived the interaction with the photodetachment laser, is detected with a microchannel plate.

The two-dimensional tomography scans are performed under the same experimental conditions as in [20]. A free-running continuous wave diode laser at 661.9 nm (Mitsubishi ML1J27, 100 mW, spectral width 0.7 nm FWHM) has been employed. It is imaged into the trap and scanned in the (x, y) plane, perpendicular to the symmetry axis of the trap, by moving the imaging lens on a mesh with 0.25 mm point spacing with a computer-controlled two-dimensional translation stage. The mesh spacing is comparable to the $1/e^2$ radius of the laser in the trap of 350 μm. For each laser position the photodetachment depletion rate is obtained in a storage time interval of 0.2–2 s by fitting an exponential decay to the ion current signal, reduced by typically 1% due to the background loss rate. The data are averaged over typically 4–8 scans. Within each scan, the mesh points are accessed in random order to avoid systematic drifts.

3. Tomography of the trapping potential

Figure 1(a) shows a tomography scan of OH^- anions in the 22-pole trap at 300 K with the rf amplitude set to 160 V. The figure also contains the sketched arrangement of the trap's copper housing mounted on the coldhead of the cryostat, the position of the 22 rf electrodes and the axial end electrodes. Figure 1(b) is a zoom of the scan which more clearly shows the measured ion density distribution. Every pixel of the histogram here represents a fitted photodetachment depletion rate $k(x, y)$ (see section 2) and is proportional to the single-particle probability density $\rho(x, y)$ along a column parallel to the z-axis. As can be seen the ion distribution as a first approximation can be considered circularly symmetric and constant in the centre region of the trap, whereas it drops to zero when the ions reach the outer regions of the trapping volume. This distribution directly visualizes the overall storage properties of a 22-pole ion trap with a flat potential in the centre and steep walls. Note that the ion density drops to zero already for smaller radii than the end electrode (the solid line in figure 1(b)), indicating that clipping of the laser at the end electrode does not affect the measured density distribution. For smaller rf amplitudes the ion density distribution would extend to larger radii and could not be fully probed by the photodetachment tomography. For this reason, we have restricted ourselves to large enough rf amplitudes in this study.

In figure 1(c), a horizontal cut through the ion distribution is shown. While in the centre the distribution is relatively uniform, the population is locally enhanced by up to 40% near the edge of the ion distribution. Such behaviour has already been observed in previous measurements [19]. To study this here in more detail, the effective potential $V(x, y)$

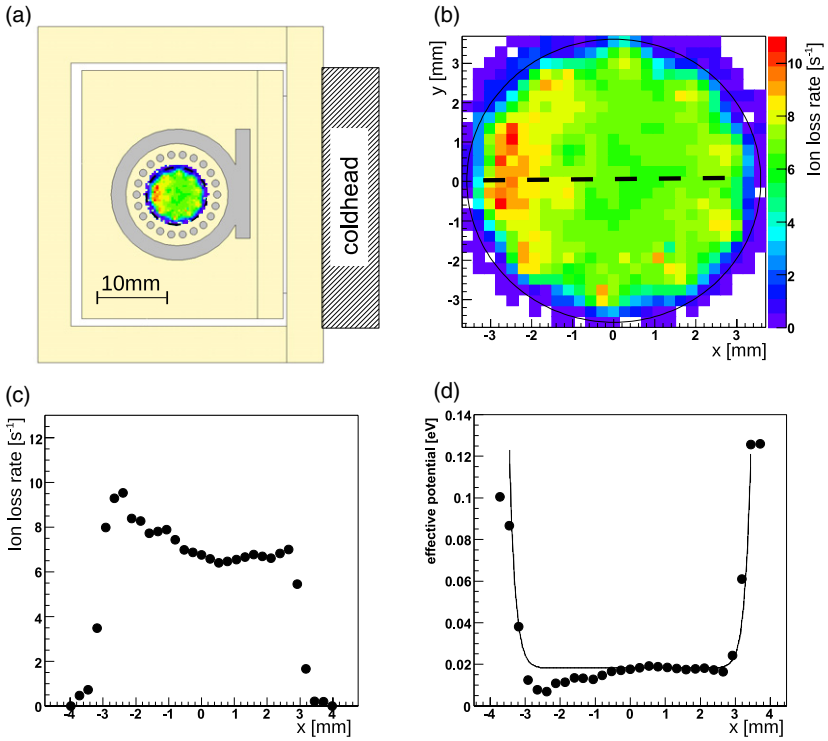

Figure 1. (a) Measured density distribution of trapped OH^- ions at 300 K buffer gas temperature with the rf amplitude set to 160 V. The sketched geometry shows the layout of the ion trap, viewed along its symmetry axis. It includes the copper housing, the 22 rf electrodes (end on), a surrounding shaping electrode and the end electrodes. (b) Zoom into the measured ion density distribution, each pixel represents an individual decay rate measurement. (c) One-dimensional cut through the density distribution along the horizontal axis. (d) Effective potential derived from the density distribution by assuming a Boltzmanm distribution of the trapped ions at 300 K.

is extracted from the local ion density $\rho(x, y)$ assuming a Boltzmann distribution for the ions in the trap:

$$\rho(x, y) = \frac{1}{Z} \exp(-V(x, y)/k_B T), \tag{6}$$

where T is the absolute temperature, k_B is Boltzmann's constant, and Z is the partition function. Since only the column density is measured, the resulting potential $V(x, y)$ is an average over the z-direction. Figure 1(d) shows a cut through the obtained effective potential for the distribution of figure 1(c). Overall, this potential compares well with the calculated potential of an ideal 22-pole potential (solid line), obtained without any free parameters from equation (2). Closer inspection reveals interesting features in the potential that deviate from the ideal multipole. While the potential is relatively flat in the centre, it shows a distinct minimum of about 12 meV near the left edge of the ion distribution and a weaker minimum of about 5 meV near its right edge. It can be excluded that this change of the distribution is caused by space charge effects, because the experiments are performed with only a few hundred ions in a trap volume of about 1 cm^3.

The same features of the effective potential are observed in measurements at a lower trap temperature. Figure 2(a) shows a tomography scan at 170 K and the same rf amplitude as above. The ion distribution again looks circular symmetric with a distinct cutoff when the ions reach the steep walls of the trapping potential. A horizontal cut through the effective potential, obtained in the same fashion as figure 1(d), is shown in figure 2(b). The same minima as for 300 K are observed in the effective potential. At this lower temperature the two minima are better resolved and appear similar in depth on the left side and slightly deeper on the right side of the potential as compared to the 300 K tomography.

A further substructure becomes visible in the 170 K density distribution. Ten clearly separated maxima in the density distribution appear almost equally spaced in angle at a radial position of about 3 mm. According to equation (6) they correspond to ten localized minima in the trapping potential at this radius with a typical depth of 10 meV. These minima have not been significant in the 300 K ion distribution at 160 V rf amplitude. They become visible, however, for larger amplitudes. Figure 3(a) shows a 300 K ion distribution for an rf amplitude of 270 V. It reveals the same ten density maxima and respective potential minima that could only be resolved at lower temperature at 160 V.

We have studied the dependence of the depth of the ten potential minima on the rf amplitude at 300 K. The depth of the deepest minimum is plotted in figure 3(b). Since the effective potential is expected to depend quadratically on the rf amplitude, a fit with only a constant and a quadratic term is applied to the data (the solid line in figure 3(b)). It yields an rf-independent offset of about 11 meV, which is attributed to the static potential of the end electrodes of the ion trap. These end electrodes produce a radially repulsive potential inside the trap, as discussed in [19, 21]. It compares well with simulations, as shown in the following section. The ten 'pockets' in the

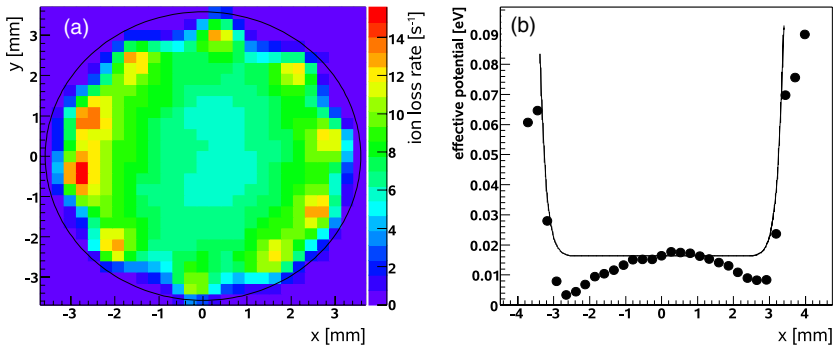

Figure 2. (a) Ion density distribution at 170 K with an rf amplitude of 160 V. It shows a substructure of ten clearly distinct maxima. (b) Cut through the effective potential, derived from the density distribution. Overall, the potential is in accordance with the effective potential of an ideal 22-pole (solid line).

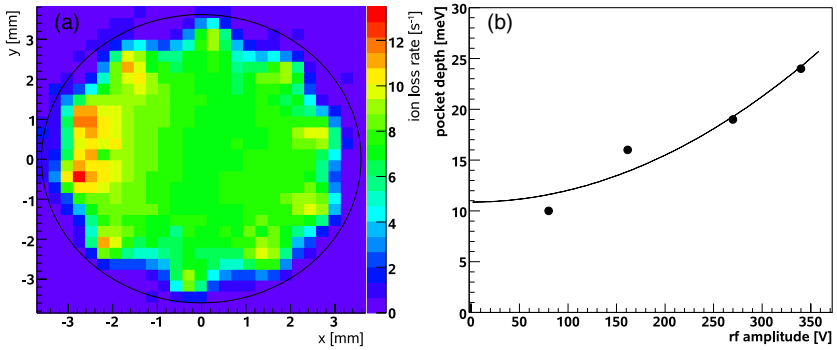

Figure 3. (a) Ion density distribution at 300 K with an rf amplitude of 270 V. The histogram shows ten distinct maxima, which correspond to minima in the effective potential. (b) The depth of the deepest minimum shows a strong increase as a function of the applied rf amplitude. The solid line shows a polynomial fit with only a constant and a quadratic term.

potential, however, reveal a more complex deviation from the ideal multipole description of equation (2). An explanation for them will also be discussed in the following section.

4. Modelling trapping potentials of realistic multipoles

The effective potential of a $2n$-pole has a $2n$-fold rotational symmetry, when averaging over one radiofrequency period. The appearance of the ten observed potential minima is therefore a clear indication for a breaking of the ideal symmetry. To investigate this effect further, the effective potential of the employed 22-pole trap has been modelled using a numerical simulation package based on a fast multipole solver [22, 23] for the boundary element problem in combination with accurate field evaluation in free space. With this method, the electric field $E(r)$ can be calculated at any location inside the trap. It is converted into the effective trapping potential using equation (1). We have verified that the simulation of the trapping potential of an ideal 22-pole structure reproduces the effective potential of equation (2) on the numerical level of accuracy.

Different assumptions have been tested as the origin of the observed ten potential minima, such as the influence of the shape and position of the end electrodes and of the copper housing around the trap electrodes, without showing a measurable effect on the potential. This suggests that imperfections of the trap geometry itself may be responsible. To simulate these imperfections a breaking of the ideal symmetry is introduced by displacing one half of the 22 radiofrequency electrodes by a small angle (see the inset in figure 4(a)). Such a small tilt of one set of electrodes against the others occurs to be the most likely displacement during the trap assembly. Upon tilting one set of electrodes by only a few tenths of a degree, the calculated effective potential of a 22-pole trap at 160 V rf amplitude and −2 V on the end electrodes immediately shows ten potential minima.

In figure 4(a) the dependence of the maximum pocket depth on the tilt angle, as obtained from a series of simulations, is plotted. These simulations have been carried out for 160 V rf amplitude. Here, an imperfection in the parallelity of only 0.2° causes a pocket depth of 5 meV. The pocket depth is calculated at each angle with and without a potential of −2 V applied to the static end electrodes. The end-electrode voltage produces an overall quadrupole potential that pushes the ion ensemble towards larger radii in the trap in addition to the tilt-induced pockets. Both data sets, with and without the end-electrode potential, are described by the same quadratic increase. For the simulations with end-electrode potential a constant offset of about 9 meV is obtained, in fair agreement with the experiment value of about 11 meV.

From the measured depths of the potential minima (figure 3(b)) a value between 3 and 5 meV is extracted for an rf amplitude of about 160 V, after subtracting the influence

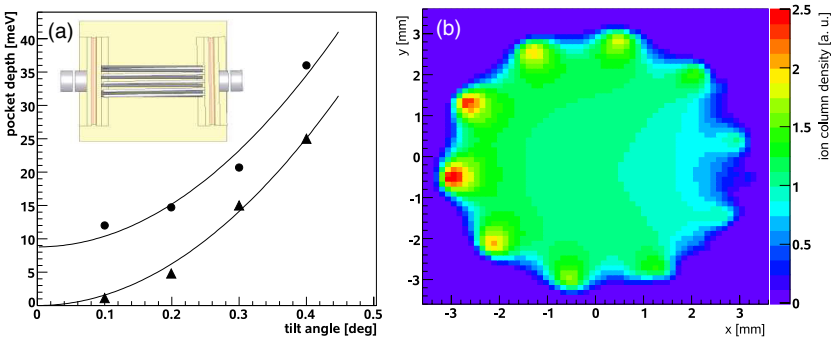

Figure 4. (a) Depth of the deepest potential minimum as a function of the tilt angle of the rf electrodes with a potential applied to the end electrodes (upper points) and without any potential on the end electrodes (lower points). The solid lines show quadratic fits without a linear term. The inset shows the geometry of the 22-pole ion trap, viewed in the direction onto the coldhead (see figure 1(a)). The right wall of the trap together with the 11 implanted rf electrodes has been tilted by an angle of 1.0°. (b) Calculated ion density distribution for 300 K in the effective potential of 270 V rf amplitude and −2 V static end electrode potential. A tilt angle of 0.15° is chosen, which leads to good agreement with the measured density distribution shown in figure 3(a).

of the static end electrode (see figure 3(b)). Such an rf-induced pocket depth is obtained in the simulation for a tilt angle between 0.15° and 0.2° (see figure 4(a)). Figure 4(b) shows a simulated density distribution for a tilt angle of 0.15°. Following equation (6), the simulation has been performed for OH^- ions that are stored at 300 K in the 22-pole trap with 270 V rf amplitude and −2 V potential on the end electrodes. This simulated density distribution agrees well with the measured distribution of figure 3(a), which has been obtained with the same trap parameters. A larger tilt angle was found to already overestimate the ten potential minima. Note that it is preferable to compare graphs of the density distributions of simulation and experiment instead of effective potentials, because the experimental potential is obtained by a logarithm of the density distribution which suppresses the fine details in the images.

When the 22-pole trap was assembled the strong influence of small displacements of the rf electrodes on the effective potential was not known. A tilt of one set of rf electrodes by a tenth of a degree can therefore not be excluded for our trap. Such small tilt angles already come close to the mechanical tolerances for the assembly of a 22-pole trap in the presently used design. This shows the need to significantly improve the precision in the rf electrode geometry when a potential with pocket depths in the μeV range is desired.

In searching for an explanation for the observed ten minima, we have extended the electric field simulations to multipoles of different order n. These calculations have shown that the number of minima observed in the effective potential of a distorted multipole ion trap is directly connected to the multipole order as $N_{\mathrm{minima}} = n - 1$. Besides the above-discussed tilt of one set of electrodes, other distortions of the ion trap, such as a parallel displacement of one set of rf electrodes, also introduces $n - 1$ minima. The number of minima therefore seems to be a general consequence of breaking the symmetry of a multipole ion trap. We expect the minima to be related to the points in space where the superimposed time-dependent electric field of the individual multipole electrodes cancels, because according to equation (1) these are the global minima of the effective potential. For a perfectly symmetric multipole trap, cancellation is expected only in the trap centre, but for a distorted symmetry several such points are found at larger radii.

5. Conclusion

In this paper, we report on a method to directly measure the column density distribution of ions in a 22-pole ion trap using photodetachment of stored OH^-. The two-dimensional tomography scans yield the effective potential averaged over the length of the trap. The measurements quantitatively confirm the overall validity of the effective potential of a 22-pole ion trap, which scales as r^{20}. For large rf amplitudes, however, new features in the potential have been observed in the form of ten almost equally spaced potential minima. These minima arise from the breaking of the 22-fold symmetry of the trap. They can be quantitatively explained by a slight tilt of half of the multipole rf electrodes within their mechanical tolerances. Also for other multipole ion traps simulations show $n - 1$ minima in the effective trapping potential as a consequence of a broken symmetry of the trap.

This observation, which has become possible due to the high sensitivity of our photodetachment tomography scans, has implications for other spectroscopic experiments in 22-pole ion traps. In particular at cryogenic temperatures, trapped ions will reside predominantly in the ten pockets of the potential. Correspondingly, the ion density along the symmetry axis of the trap would become very small, and only a small spectroscopic signal would be detected for a laser beam pointing along the trap axis. Further studies are needed to find out if ions that reside in the ten pockets may be subject to enhanced radiofrequency heating, similar to the influence of the static end electrode potential, which can increase the translational temperature by a few kelvin [21]. Generally, it is therefore advisable to operate the ion trap at rf amplitudes far below 100 V to significantly suppress the pockets. To overcome the pockets a significantly enhanced precision in the manufacturing and assembly of 22-pole traps is required. An interesting alternative for precisely controllable multipole ion traps are planar, chip-based traps [24].

Acknowledgments

We thank Ferdinand Schmidt-Kaler for helpful discussions. This work is supported by the Deutsche Forschungsgemeinschaft under contract no WE 2592/2-1. PH acknowledges support by the Alexander von Humboldt foundation. KS acknowledges support by the European commission within EMALI (contract no MRTN-CT-2006-035369) and the Landesstiftung Baden-Württemberg in the framework atomics (contract no PN 63.14) and the Eliteprogramm Postdoktorandinnen und Postdoktoranden.

References

[1] Gerlich D 1992 *Adv. Chem. Phys.* **82** 1
[2] Gerlich D 1995 *Phys. Scr.* T **59** 256
[3] Schlemmer S, Kuhn T, Lescop E and Gerlich D 1999 *Int. J. Mass Spectrom.* **185–7** 589
[4] Schlemmer S, Lescop E, von Richthofen J, Gerlich D and Smith M A 2002 *J. Chem. Phys* **117** 2068
[5] Mikosch J, Kreckel H, Wester R, Plasil R, Glosik J, Gerlich D, Schwalm D and Wolf A 2004 *J. Chem. Phys.* **121** 11030
[6] Asvany O, Kumar P, Redlich B, Hegemann I, Schlemmer S and Marx D 2005 *Science* **309** 1219–22
[7] Glosík J, Hlavenka P, Plašil R, Windisch F, Gerlich D, Wolf A and Kreckel H 2006 *Phil. Trans. R. Soc.* A **364** 2931
[8] Boyarkin O V, Mercier S R, Kamariotis A and Rizzo T R 2006 *J. Am. Chem. Soc.* **128** 2816
[9] Dzhonson A, Gerlich D, Bieske E J and Maier J P 2006 *J. Mol. Struct.* **795** 93–7
[10] Kreckel H, Bing D, Reinhardt S, Petrignani A, Berg M and Wolf A 2008 *J. Chem. Phys.* **129** 164312
[11] Asvany O, Savic I, Schlemmer S and Gerlich D 2004 *Chem. Phys.* **298** 97–105
[12] Asvany O, Schlemmer S and Gerlich D 2004 *Astrophys. J.* **617** 685–92
[13] Otto R, Mikosch J, Trippel S, Weidemüller M and Wester R 2008 *Phys. Rev. Lett.* **101** 063201
[14] Wester R 2009 *J. Phys. B: At. Mol. Opt. Phys.* **42** 154001
[15] Dehmelt H G 1967 *Adv. At. Mol. Phys.* **3** 53
[16] Schubert M, Siemers I and Blatt R 1989 *J. Opt. Soc. Am.* B **6** 2159
[17] Walz J, Siemers I, Schubert M, Neuhauser W, Blatt R and Teloy E 1994 *Phys. Rev.* A **50** 4122
[18] Mikosch J, Frühling U, Trippel S, Otto R, Hlavenka P, Schwalm D, Weidemüller M and Wester R 2008 *Phys. Rev.* A **78** 023402
[19] Trippel S, Mikosch J, Berhane R, Otto R, Weidemüller M and Wester R 2006 *Phys. Rev. Lett.* **97** 193003
[20] Hlavenka P, Otto R, Trippel S, Mikosch J, Weidemüller M and Wester R 2009 *J. Chem. Phys.* **130** 061105
[21] Asvany O and Schlemmer S 2009 *Int. J. Mass. Spectrom.* **279** 147
[22] Greengard L 1988 *The Rapid Evaluation of Potential Fields in Particle Systems* (Cambridge, MA: MIT Press)
[23] Nabors K, Korsmeyer F T, Leighton F T and White J 1994 *SIAM J. Sci. Stat. Comput.* **15** 713
[24] Debatin M, Kröner M, Mikosch J, Trippel S, Morrison N, Reetz-Lamour M, Woias P, Wester R and Weidemüller M 2008 *Phys. Rev.* A **77** 033422